Fluctuations in a model ferromagnetic film driven by a slowly oscillating field with a constant bias

Gloria M. Buendía[1] and Per Arne Rikvold[2]

[1]*Department of Physics, Universidad Simón Bolívar, Caracas 1080, Venezuela*
[2]*Department of Physics, Florida State University, Tallahassee, Florida 32306-4350, USA*

We present a numerical and theoretical study that supports and explains recent experimental results on anomalous magnetization fluctuations of a uniaxial ferromagnetic film in its low-temperature phase, which is forced by an oscillating field above the critical period of the associated dynamic phase transition (DPT) [P. Riego, P. Vavassori, and A. Berger, Phys. Rev. Lett. **118**, 117202 (2017)]. For this purpose, we perform kinetic Monte Carlo simulations of a two-dimensional Ising model with nearest-neighbor ferromagnetic interactions in the presence of a sinusoidally oscillating field, to which is added a constant bias field. We study a large range of system sizes and supercritical periods and analyze the data using a droplet-theoretical description of magnetization switching. We find that the period-averaged magnetization, which plays the role of the order parameter for the DPT, presents large fluctuations that give rise to well-defined peaks in its scaled variance and its susceptibility with respect to the bias field. The peaks are symmetric with respect to zero bias and located at values of the bias field that increase toward the field amplitude as an inverse logarithm of the field oscillation period. Our results indicate that this effect is independent of the system size for large systems, ruling out critical behavior associated with a phase transition. Rather, it is a stochastic-resonance phenomenon that has no counterpart in the corresponding thermodynamic phase transition, providing a reminder that the equivalence of the DPT to an equilibrium phase transition is limited to the critical region near the critical period and zero bias.

I. INTRODUCTION

The hysteretic response when a uniaxial spin system with long-range order (i.e., below its critical temperature) is subject to a symmetrically oscillating field of amplitude H_0 and period P depends crucially on P. If P is much longer than the response time of the system (which depends on the temperature and H_0), a symmetric hysteresis loop centered on zero results. If P is much shorter than the response time, asymmetric hysteresis loops centered around the values of the system's static order parameter are observed. Numerical studies in the 1990s showed that the transition between these two regimes is not smooth. Rather, there is a critical period P_c, where the period-averaged order parameter $\langle Q \rangle$ (see formal definition in Sec. II) vanishes in a singular fashion. This phenomenon was first observed by Tomé and de Oliveira [1] in a kinetic mean-field study of an Ising model, followed by kinetic Monte Carlo (MC) simulations by Rao, Krishnamurthy, and Pandit [2] and Lo and Pelcovitz [3]. Early work in the field was reviewed by Chakrabarti and Acharyya in Ref. [4]. Kinetic MC combined with finite-size scaling analysis [5–10], as well as further mean-field studies of Ising and Ginzburg-Landau models [11–14], confirmed not only that this is a true, dynamic phase transition (DPT), but also that it is in the same universality class as the corresponding equilibrium Ising model. The DPT has been confirmed experimentally in [Co/Pt]$_3$ magnetic multilayers [15] and uniaxial Co films [16].

With all the attention that has been given to the DPT and its universality class, one might lose sight of the fact that the equivalence between the critical properties of the equilibrium Ising model and the DPT of the same model in an oscillating field does not necessarily amount to equivalence *outside* the critical region. A warning was provided very recently by Riego, Vavassori, and Berger [17]. These authors fabricated

Co films with $(10\underline{1}0)$ crystallographic surface structure with a single, in-plane magnetic easy axis, which they subjected to a sinusoidally oscillating, in-plane magnetic field plus a constant bias field H_b. Such a constant bias field has previously been shown by MC simulations and finite-size scaling to be (at least a significant component of) the field conjugate to $\langle Q \rangle$ in the critical region near P_c [8], and this has later been confirmed for mean-field models [12–14] and in experiments [16]. It therefore seemed surprising that, in the experiments reported in Ref. [17], both the fluctuations in the order parameter and its derivative with respect to H_b, for $P \gg P_c$, behaved quite differently from the dependence of the equilibrium susceptibility on the applied static field at temperatures above critical. Instead of the wide, smooth, unimodal maximum of the supercritical equilibrium susceptibility of the Ising model, two distinct peaks were observed at nonzero values of H_b, symmetrical about zero [17]. In their article the authors also presented kinetic mean-field results that corroborate the presence of these peaks, which they dubbed "sidebands."

The purpose of the present paper is to investigate the long-period parameter regime with kinetic MC simulations of a two-dimensional Ising model with nearest-neighbor ferromagnetic interactions. To match the experimental conditions of Ref. [17] as closely as possible, we choose the oscillating field to have a sinusoidal wave form. We are not aware that systematic simulations in this regime have been performed previously. Our study reveals "sidebands" analogous to the experimental results. We thus conclusively confirm that the experimentally observed phenomenon is not caused by residual magnetostatic long-range interactions. Using simulations for a range of field periods and system sizes together with knowledge of the kinetics of magnetization switching by homogeneous nucleation and growth of antiphase droplets [18], we demonstrate that the "sidebands" result from noncritical fluctuations during the half cycles when the sign of the oscillating field is opposite to that

134306-1

of the bias field. This is essentially a stochastic resonance phenomenon [19–21].

The rest of this paper is organized as follows. In Sec. II we describe the model and details of the simulation method, and we define the appropriate observables to be measured. Our numerical results are presented in Sec. III. In Sec. III A we present numerical observation of sidebands for a single, supercritical value of the field period. In Sec. III B we present short time series of the system magnetization for several values of bias and period, which enable us to propose a simple approximation for $\langle Q \rangle$ in the limits of weak bias and long period. In Sec. III C we present numerical results for $\langle Q \rangle$ vs H_b for a wide range of supercritical periods, as well as the sideband positions H_b^{peak} as functions of period and system size. The latter are analyzed using results from the droplet theory of magnetization reversal. Our conclusions are given in Sec. IV. A short summary of pertinent results from the droplet theory of magnetization reversal is given in Appendix A, and the case of extremely long periods is discussed in Appendix B. A brief discussion of the mathematically simpler case of a square-wave oscillating field is presented in Appendix C.

II. MODEL AND MONTE CARLO SIMULATION

We consider a kinetic $S = 1/2$ Ising model with a time-dependent external field and ferromagnetic nearest-neighbor interactions. Its Hamiltonian is

$$\mathcal{H} = -J \sum_{\langle ij \rangle} s_i s_j - [H(t) + H_b] \sum_i s_i, \qquad (1)$$

where $J > 0$, $s_i = \pm 1$, the first sum runs over all nearest-neighbor pairs, and the second one over all sites. H_b is a constant "bias field," and $H(t)$ is a symmetrically oscillating external field of period P. Here we choose

$$H(t) = H_0 \cos\left(\frac{2\pi}{P} t\right). \qquad (2)$$

The system is simulated on a square lattice of $N = L \times L$ sites with periodic boundary conditions. We perform Glauber single-spin-flip dynamics in a heat bath at temperature T. A spin at a randomly chosen site i is allowed to flip from s_i to $-s_i$ with probability

$$W(s_i \to -s_i) = \frac{1}{1 + \exp(\beta \Delta E_i)}, \qquad (3)$$

where ΔE_i is the change in the system energy associated with flipping the spin i, and $\beta = 1/k_B T$ where k_B is Boltzmann's constant. The time unit is one MC step per site (MCSS), during which, on average, each site is visited once. Hereafter, H_0, H_b, and T are all given in units of the interaction constant J (i.e., $J = k_B = 1$), and P is given in units of MCSS.

The Glauber dynamic can be derived as the weak-coupling limit of the quantum-mechanical Hamiltonian of a collection of quasifree Fermi fields in thermal equilibrium with a heat bath [22]. However, the DPT with $H_b = 0$ has been shown to be universal with respect to dynamics that obey detailed balance in equilibrium, including Metropolis [23] and "soft Glauber" [9], as well as different forms of $H(t)$ including square wave [7,9] and sawtooth [15].

We calculate the time-dependent, normalized magnetization per site,

$$m(t) = \frac{1}{L^2} \sum_i s_i(t), \qquad (4)$$

and by integrating it over each cycle of the magnetic field, we obtain the average magnetization during the kth cycle of the field,

$$Q_k = \frac{1}{P} \int_{(k-1)P}^{kP} m(t) dt. \qquad (5)$$

The dynamic order parameter of the model is the period-averaged magnetization, $\langle Q \rangle$, defined as the average of Q_k over many cycles. Its fluctuations are measured by the scaled variance,

$$\chi_L^Q = L^2 (\langle Q^2 \rangle - \langle Q \rangle^2), \qquad (6)$$

and its dependence on the bias field is measured by the susceptibility with respect to H_b,

$$\chi_L^b = d\langle Q \rangle / dH_b. \qquad (7)$$

In order to take advantage of temperature and field-dependent parameters measured with high precision in previous MC simulations [6], our calculations are performed with $H_0 = 0.3$ at $T = 0.8 T_c$, where $T_c = 2/\ln(1 + \sqrt{2}) \approx 2.269$ is the critical temperature of the standard, square-lattice Ising model in zero field. In the absence of a bias field, at this temperature, and for sufficiently large L, switching between the equilibrium values of m, following field reversal from $-H_0$ to $+H_0$, occurs via a nearly deterministic and L-independent multidroplet mechanism [18]. In Ref. [6], the characteristic switching time scale (the time from the field reversal until the system magnetization reaches zero) under Glauber dynamics with the same parameters as we use here was measured by MC simulations as $\tau_0 \approx 74.6$. In the same work, the critical period in a sinusoidal field of amplitude H_0 with zero bias was measured as $P_c \approx 258$.

The cycle-averaged magnetization $\langle Q \rangle$ vanishes for $P \gtrsim P_c$ and $H_b = 0$. Near criticality, the constant bias field H_b is the field conjugate to $\langle Q \rangle$, and the period P mimics the temperature in the equilibrium phase transition. Simulations were performed for periods between $P = 258$ and 28 000 and system sizes between $L = 32$ and 1024. Except for the smallest values of P, the measurements were obtained by averaging over 800 field cycles, after discarding 200 cycles. This means that at least $800 \times P$ MCSS were performed for each measurement.

III. NUMERICAL RESULTS AND ANALYSIS

A. Observation of "sidebands"

Results of simulations with $P = 1000 \approx 3.9 P_c$ for several values of L are displayed in Fig. 1. "Sidebands" are observed, consistent with the experiments reported in Ref. [17]. The dependence of the order parameter $\langle Q \rangle$ on the bias H_b is shown in Fig. 1(a). For weak H_b, $\langle Q \rangle$ increases almost linearly with H_b, but the slope of the curve increases considerably around $|H_b| \approx 0.09$, followed by saturation of $\langle Q \rangle$ for $|H_b| \gtrsim 0.15$. This behavior is reflected in the bimodal shape of
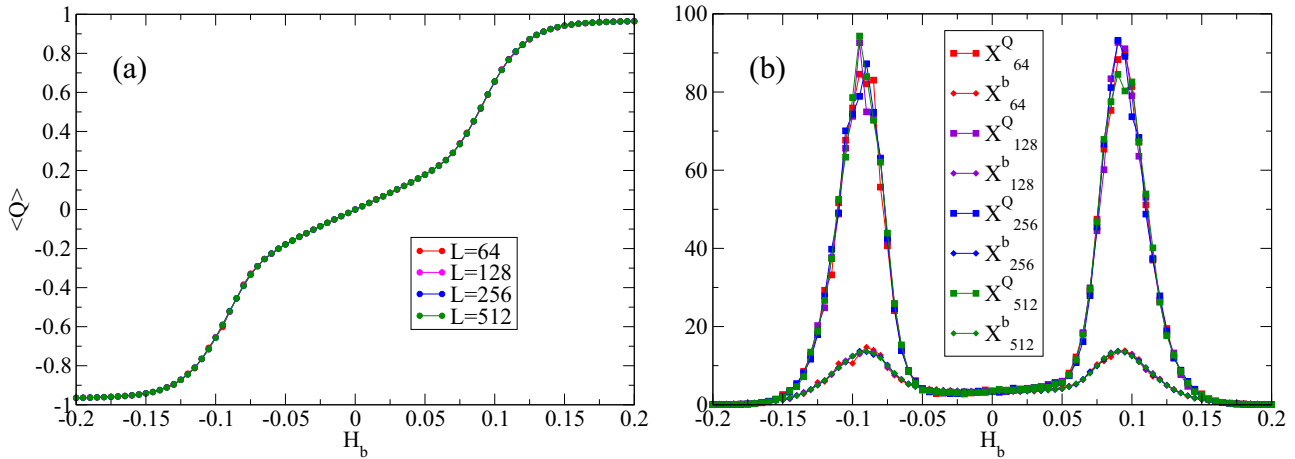
FIG. 1. Results with $P = 1000 \approx 3.9 P_c$ for system sizes $L = 64$, 128, 256, and 512. With this period length and range of system sizes, finite-size effects are negligible, and the curves for different system sizes practically coincide. (a) The order parameter $\langle Q \rangle$ vs H_b. Error bars are smaller than the symbol size. (b) The scaled variance χ_L^Q and susceptibility χ_L^b. See discussion of this figure in Sec. III A.

the susceptibility χ_L^b, shown by the lower set of curves in Fig. 1(b). Between the two peaks lies a flat-bottomed valley corresponding to the linear regime in part (a), and a rapid approach to zero for large $|H_b|$ mirrors the saturation of $\langle Q \rangle$ also seen in (a). The scaled variance χ_L^Q also displays peaks, whose positions coincide with those of χ_L^b. However, the ratio χ_L^Q / χ_L^b for fixed P depends quite strongly on H_b with maximum values near the peaks. This variable ratio precludes a straightforward interpretation in terms of an effective, nonequilibrium fluctuation-dissipation relation with P playing the role of "temperature." For these values of L and P, finite-size effects are seen to be negligible, ruling out critical behavior associated with a phase transition. The relationships between system size, field period, and finite-size effects will be discussed in further detail below.

B. Magnetization time series

To gain a more detailed understanding of the relationships between bias, period, system size, and the order-parameter fluctuations, we present in Fig. 2 short time series of the normalized magnetization, $m(t)$. The total applied field, $H(t) + H_b$, is shown as an orange curve. In this figure we set $H_b > 0$, so that the up-spin phase is favored and the down-spin phase is disfavored.

Figure 2(a) shows data for $P = 1000$ and $H_b = +0.10$, just on the strong-bias side of the fluctuation peak for this period length. For the smaller system sizes ($L = 32$ and 64), the switching from the favored (up-spin) to the disfavored (down-spin) magnetization is stochastic and abrupt (mediated by a single or a few droplets of the down-spin phase [18]) and occurs only in narrow time windows near the negative extrema of the total applied field. For the larger systems, the switching becomes more deterministic and gradual (multidroplet [18]). However, the growing down-spin phase does not have time to completely fill the system before the field again becomes positive. For the largest system studied, $L = 1024$, the extreme negative magnetizations during a period are close to -0.2.

Figure 2(b) shows data for $P = 1000$ and $H_b = +0.0915$, at the maximum of the fluctuation peak. The switching

behavior for $L = 32$ remains stochastic. However, the larger systems appear more deterministic, and their extreme negative magnetizations during a period are close to -0.4.

Figure 2(c) shows data for $P = 1000$ and $H_b = +0.08$, just on the weak-bias side of the fluctuation peak. The switching for $L = 32$ remains stochastic. The larger systems behave more deterministically, and the extreme negative magnetizations during a period approach -0.8.

These results illustrate how the switching behavior in the peak region crosses over from a stochastic single-droplet mechanism for small L to a nearly deterministic multidroplet mechanism for larger L, in agreement with known results for field-driven magnetization switching by homogeneous nucleation and growth of droplets of the stable phase [18].

Figure 2(d) shows data for $L = 128$ with a weak bias, $H_b = +0.04$, and two different period lengths, $P = 1000$ and 14 000. In both cases, the switching is nearly deterministic and complete, so that the period-averaged magnetization $\langle Q \rangle$ depends mostly on the relative amounts of time the system spends in the two phases. As P increases, the switching occurs earlier in the half-period.

The differences between the single-droplet and multidroplet switching modes are further illustrated in Fig. 3. In Fig. 3(a), time series for $m(t)$ over five cycles with $P = 1000$ at the corresponding peak position, $H_b^{\text{peak}} = +0.0915$, show data for $L = 32$ and 1024. All the parameters are the same as in Fig. 2(b), except the seed for the random number generator. When the total applied field, $H(t) + H_b$, is negative, the down-spin phase, which is disfavored by the positive bias, is the equilibrium phase. Nucleation and growth of this phase may only occur during the time intervals of negative total applied field. Snapshots captured at $m(t) = +0.1$ during these growth periods, corresponding to a down-spin fraction of 0.45, are shown in Fig. 3(b) for $L = 32$ and in Fig. 3(c) for $L = 1024$.

For $L = 32$ we see a single down-spin droplet which, as seen from the time series in Fig. 3(a), nucleated during the third period shown, near the time when the field had its largest negative value. It barely reached the capture threshold of $m = +0.1$ before the field again became positive and caused it to decay. The stochastic nature of this single-droplet switching
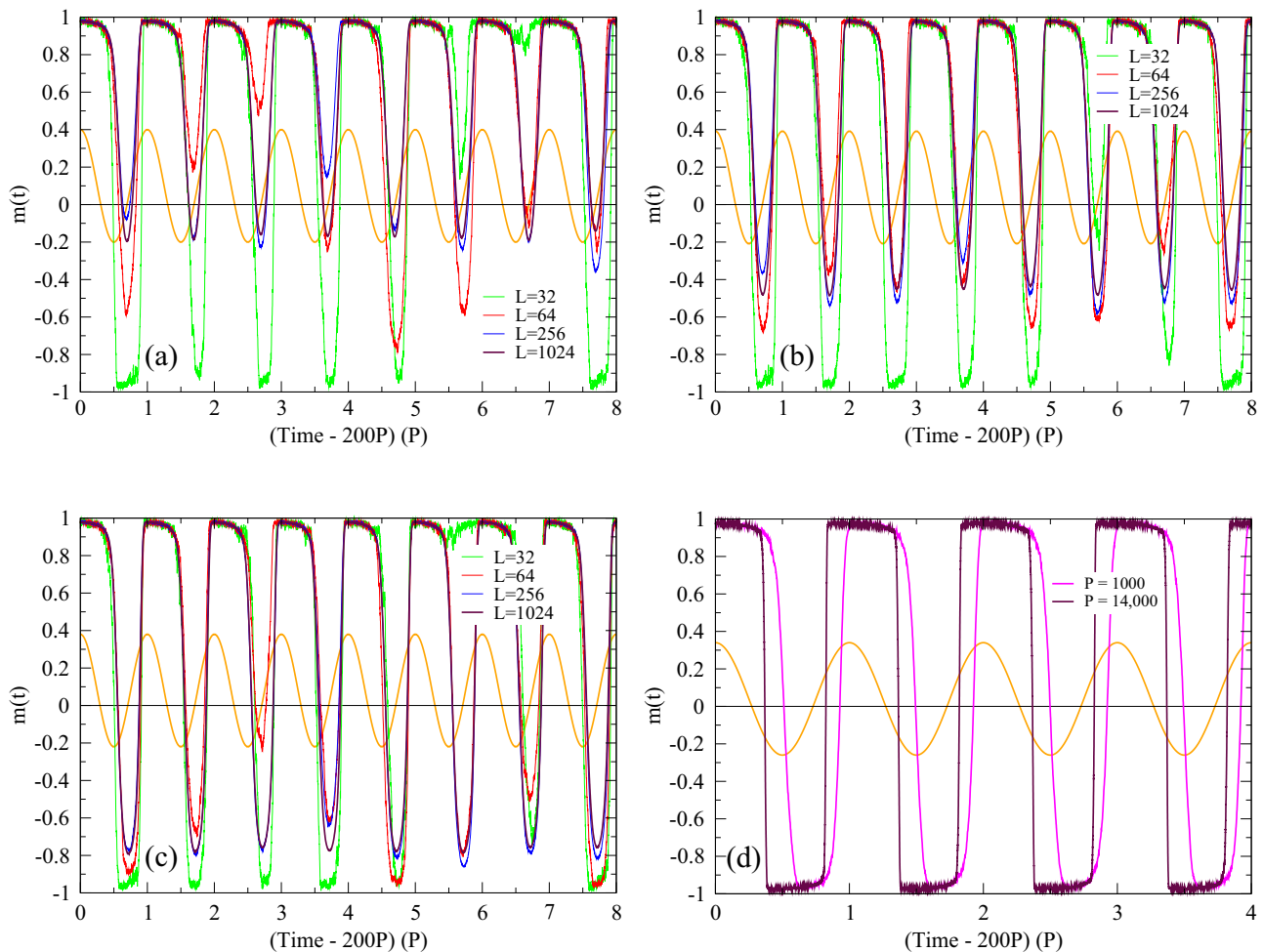
FIG. 2. The time-dependent magnetization $m(t)$ over a few cycles following a $200P$ stabilization run, using systems with L between 32 and 1024. In all four parts, the bias is positive, and the total applied field, $H(t) + H_b$, is shown as an orange cosine curve. A detailed discussion of this figure is given in Sec. III B. (a) $P = 1000$ and $H_b = +0.10$, just on the strong-bias side of the fluctuation peak for this period length. (b) $P = 1000$ and $H_b = +0.0915$, at the maximum of the fluctuation peak. (c) $P = 1000$ and $H_b = +0.08$, just on the weak-bias side of the fluctuation peak. (d) $L = 128$ and a weak bias $H_b = +0.04$ with two different period lengths, $P = 1000$ and $14\,000$. The switching is nearly deterministic and complete, and as P increases, it occurs earlier in the half-period. This observation suggests the asymptotic weak-bias, long-period approximation for $\langle Q(H_b/H_0)\rangle$, given in Eq. (9) and included in Fig. 4(a).

mode is also clearly reflected by the time series. During the five periods shown, the capture threshold was only reached twice. And only once, during the fifth period, do we see full saturation of the down-spin phase before the field again becomes positive.

For $L = 1024$ the picture is quite different. In the snapshot we see a large number of growing clusters that have nucleated at different times during the negative-field time interval. Some of these have already coalesced by the time the snapshot was captured, while others are still growing independently. From the time series it is seen that this multidroplet switching mode leads to a nearly deterministic evolution of the total magnetization, with the underlying stochasticity only evident in the slight variations of the minimum magnetization values from period to period. This switching process is well described by the Kolmogorov-Johnson-Mehl-Avrami (KJMA) approximation [18,24–28].

Magnetization reversal from the favored to the disfavored direction is only possible while the total applied field, $H(t) + H_b$, has the opposite sign of the bias, H_b. This implies that $-1 < H_b/H(t) \leqslant 0$. Switching from the favored phase to the disfavored one on average takes longer time than switching in the opposite direction. Thus, the time the system can spend in the disfavored phase during each period must be less than or equal to the time that the field has the disfavored direction,

$$t_{\text{Dmax}} = \frac{P}{2}\left[1 - \frac{2}{\pi}\sin^{-1}\left(\frac{|H_b|}{H_0}\right)\right]. \tag{8}$$

In this limit of long period and weak bias, $\langle Q\rangle$ is simply determined by the sign of H_b and the difference between the fractions of the period that the total field has the same and the opposite sign as H_b, respectively. This yields

$$\langle Q\rangle \approx \frac{2m_0}{\pi}\sin^{-1}\left(\frac{H_b}{H_0}\right), \tag{9}$$

which is symmetric under simultaneous reversal of H_b and $\langle Q\rangle$. Here, m_0 is the magnitude of the magnetization in the favored phase. This approximation represents a lower bound on the magnitudes of $\langle Q\rangle$ and χ^b [29]. The former is included
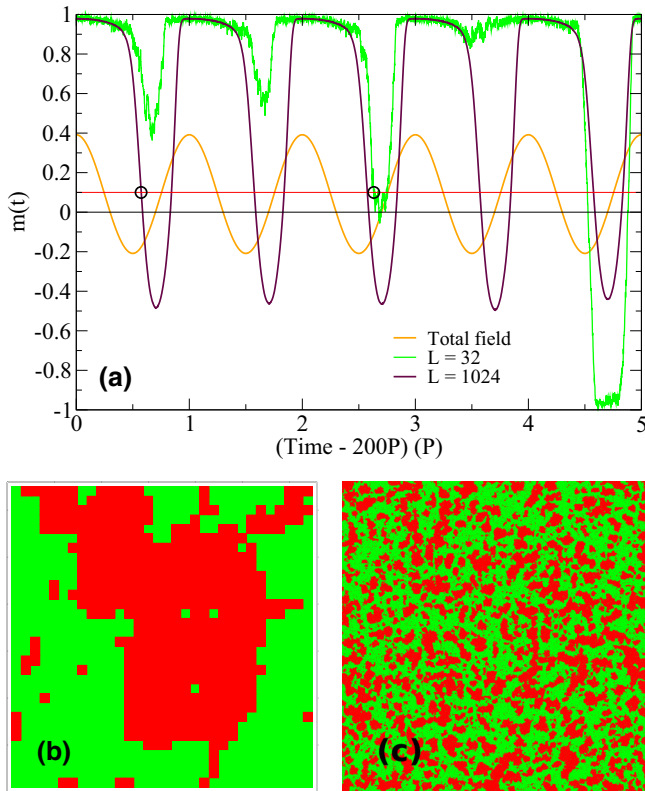
FIG. 3. A short time series and snapshots showing growing disfavored-phase clusters for $P = 1000$ at the corresponding peak position, $H_b^{peak} = +0.0915$. (a) Time series $m(t)$ over five cycles following a $200P$ stabilization run, showing data for $L = 32$ (green) and 1024 (maroon). The total applied field, $H(t) + H_b$, is shown as an orange cosine curve. The snapshots were captured the first time past $200P$ that $m(t)$ fell below $+0.1$ (red horizontal line in the figure), corresponding to a disfavored-phase (down-spin) fraction of 0.45. The times of capture are marked by black circles. In the following snapshots, regions of the up-spin phase are green, and down-spin are red. (b) $L = 32$. A single droplet of the down-spin phase has nucleated near the time when the total applied field has its largest negative value. The highly stochastic nature of the single-droplet switching mode is also evident from the time series in part (a). (c) $L = 1024$. Many droplets of the down-spin phase have nucleated at different times and then grown almost independently. At the moment of capture, some clusters have coalesced while others are still growing independently. From the time series in part (a) it is seen that this multidroplet switching mode leads to a nearly deterministic evolution of the total magnetization. This figure is further discussed in Sec. III B.

as a dashed curve in Fig. 4(a). However, the bounds depend on the wave form of the oscillating field, and as we show in Appendix C, they vanish in the case of a square-wave field.

The corrections to this approximation are of $O(t_{FD}(H_b, H_0)/P)$, where $t_{FD}(H_b, H_0)$ is the average time it takes the magnetization to switch to the disfavored direction, *after* the total applied field has changed sign. For $|H_b| \ll H_0$, the correction vanishes as $1/P$, as seen in Fig. 4(a). However, for larger $|H_b|$, $t_{FD}(H_b, H_0) \sim P$, and the "correction" becomes the dominant part of $\langle Q \rangle$, determining the sideband peak positions, H_b^{peak}. The details are discussed below in Sec. III C.

C. Dependence on H_b, P, and L

Results for $L = 128$ and a range of periods between $P_c = 258$ and $P = 28{,}000$ are shown in Fig. 4. In the critical region, H_b is the field conjugate to $\langle Q \rangle$ [8,12–14,16]. At $P = P_c$, $\langle Q \rangle$ therefore vanishes in a singular fashion as H_b approaches zero. On the scale of Fig. 4(a), this singularity appears as a jump in $\langle Q \rangle$ at $H_b = 0$ for $P = P_c$, resulting in very narrow central peaks in both χ_L^b and χ_L^Q. We also found broad central peaks in both quantities for $P = 400$, which are due to finite-size broadening of the critical region for this relatively modest system size. For clarity, these central peaks are not included in Fig. 4(b). Beyond $P = 500$, $\langle Q \rangle$ becomes linear for small H_b, with a slope that approaches that of the asymptotic approximation in Eq. (9) as P increases. Simultaneously, the peaks in χ_L^b and χ_L^Q increase in height, and their positions H_b^{peak} move in the directions of $\pm H_0$, as seen in Fig. 4(b). [For clarity, some of the values of P included in Fig. 4(a) are excluded from Fig. 4(b).]

The magnitudes of the peak positions, $|H_b^{peak}|$, are plotted vs P for different values of L in Fig. 5(a). We note two main features. First, $|H_b^{peak}|$ increases quite rapidly with P for relatively short periods, and much more slowly for longer periods. This behavior is consistent with the experimental data shown in Fig. 2 of Ref. [17]. Second, finite-size effects are essentially negligible for $P \lesssim 2000$, as already shown in Fig. 1 for $P = 1000$. For longer periods, $|H_b^{peak}|$ increases with L for smaller sizes, and then becomes size independent for larger L.

In order to explain this behavior quantitatively, we first recall from the time series shown in Fig. 2 that for bias near $|H_b^{peak}|$, the time it takes $m(t)$ to change significantly toward the disfavored sign is on the order of a finite fraction of P. For stronger bias, the total field driving the magnetization toward the disfavored sign is too weak and consequently the time required for switching is much longer than P, so that reliable magnetization reversal does not occur. For weaker bias, the field in the disfavored direction is relatively strong, and complete and reliable magnetization reversal takes place on a time scale significantly shorter than P. In other words, the peak positions correspond to bias values that produce magnetization reversal on a time scale of P. Equations for magnetization switching rates by the stochastic single-droplet mechanism that dominates for small systems [Eq. (A1)] and the nearly deterministic multidroplet mechanism that dominates for large systems [Eq. (A2)] are found in Appendix A. The nucleation rate for droplets of the disfavored phase varies very strongly with the oscillating field, having appreciable values only in a narrow window near the maximum field in the disfavored direction, $|H| = H_0 - |H_b^{peak}|$. Using this value of $|H|$ and ignoring less important prefactors, we can use these equations to write the following requirement for $|H_b^{peak}|$:

$$L^{-a} \exp\left(\frac{1}{b} \frac{\Xi_0}{H_0 - |H_b^{peak}|}\right) \sim P, \qquad (10)$$

with $a = 2$ and $b = 1$ for single-droplet switching, and $a = 0$ and $b = 3$ for multidroplet switching. The meaning of the constant $\Xi_0 \approx 0.506$ is explained in Appendix A. In either case, this equation is equivalent to a statement that $|H_b^{peak}|$
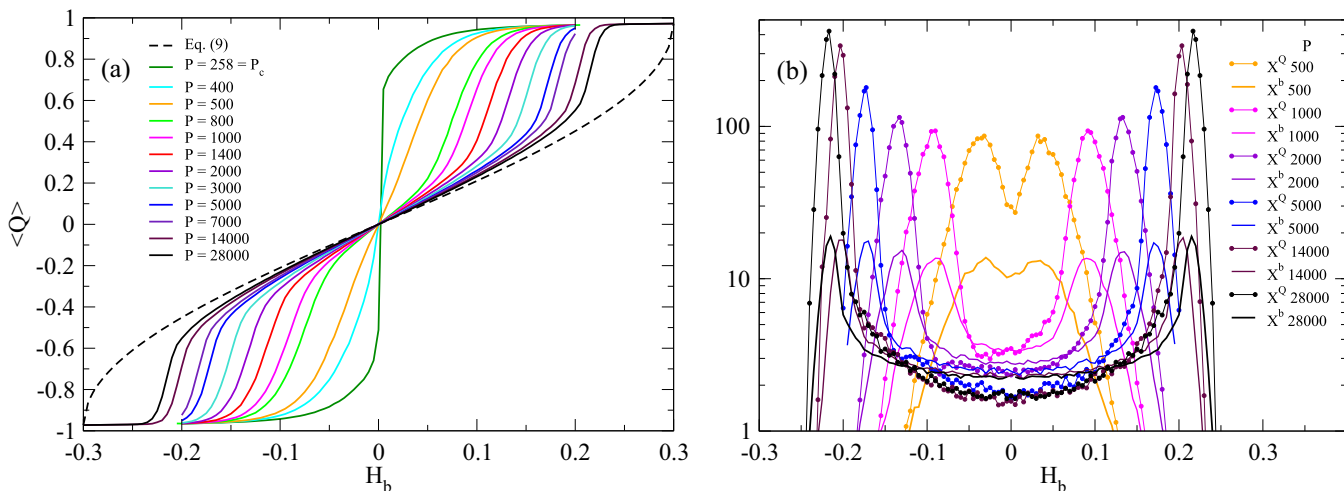
FIG. 4. Results for $L = 128$ and a range of periods between $P_c = 258$ and $P = 28{,}000$. (a) The order parameter $\langle Q \rangle$ vs H_b. Error bars are on the order of the line thickness. The dashed curve is the weak-bias, long-period approximation of Eq. (9). (b) The scaled variance χ_L^Q and the susceptibility χ_L^b vs H_b. The sideband peaks occur at values of H_b that increase with P. For clarity, data for some values of P are omitted in (b), including a narrow critical peak for $P = P_c = 258$ at $H_b = 0$ and a broad central peak for $P = 400$.

should approach H_0 asymptotically as $1/\log P$ for long periods. (A caveat to this statement for the case of extremely long periods is discussed in Appendix B.) Plotting $1/(H_0 - |H_b^{\text{peak}}|)$ vs $\log P$ therefore should produce straight lines for large values of P. The ratio between the slopes of the lines representing multidroplet switching for large L and those representing single-droplet switching for small L should be 3/1. Such a plot is presented in Fig. 5(b). The slope ratio between the curves representing $L = 256$ and $L = 32$ in the long-P regime is approximately 2.867, consistent with the theoretical prediction. This conclusion is confirmed by the short time series of $m(t)$ for $P = 20\,000$ for these two system sizes, shown in Fig. 6. In the switching regions, the smaller system displays the stochastic, square wave form characteristic of single-droplet switching [20], while the larger system shows the continuous wave form characteristic of multidroplet switching [6].

To further support our conclusions, we calculated the transition times and the order parameter in the multidroplet regime for the mathematically simpler case, in which the sinusoidally oscillating field has been replaced by a square-wave field. The details of the calculations are given in Appendix C. In Fig. 7 we show that there is very good agreement between the theoretically calculated $\langle Q \rangle$ and the simulations, particularly when $|H_b| \lesssim |H_b^{\text{peak}}|$.

IV. SUMMARY AND CONCLUSION

Riego *et al.* [17] recently presented experimental data on Co films with a single, in-plane magnetic easy axis, which were subjected to a slowly oscillating magnetic field with an added constant bias. In the present paper we have presented kinetic MC simulations and theoretical analysis of a two-
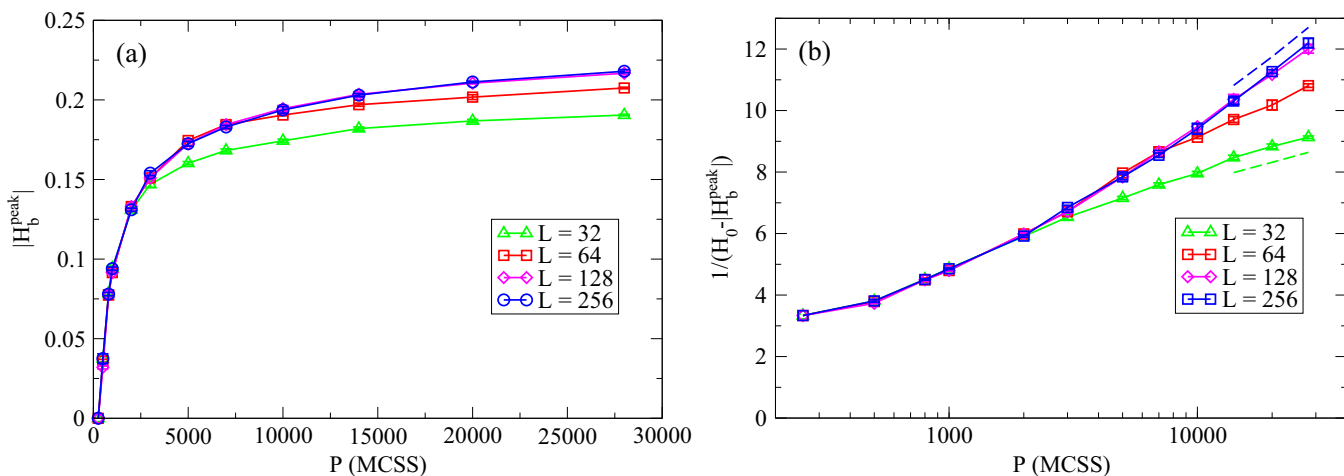

FIG. 5. Peak positions $|H_b^{\text{peak}}|$ as defined by the maxima of the scaled variance χ_L^Q, shown vs period length $P \geqslant P_c$. (a) $|H_b^{\text{peak}}|$ vs P, plotted on linear scales. (b) The peak positions plotted as $1/(H_0 - |H_b^{\text{peak}}|)$ vs $\log P$, as suggested by Eq. (10). The blue and green dashed lines represent the slopes of the curves between $P = 14\,000$ and $28\,000$ for $L = 256$ and $L = 32$, respectively. The ratio of the slopes is approximately 2.867, close to the 3/1 ratio expected from droplet theory. This figure is analogous to Fig. 2 of Ref. [18].
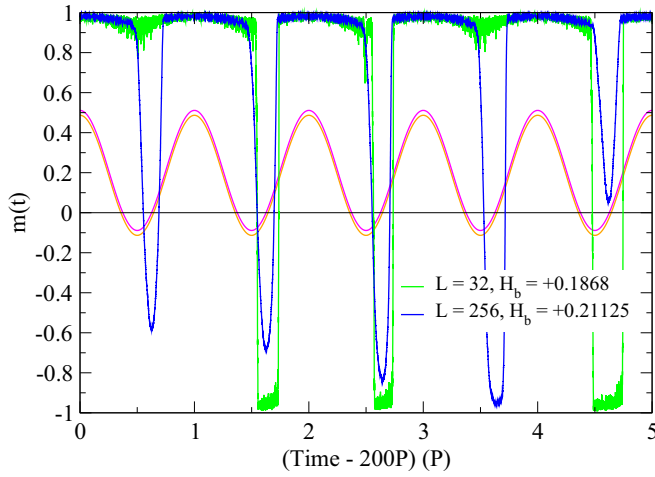
FIG. 6. Time series of $m(t)$ over five periods with $P = 20\,000$, following a $200P$ stabilization run. Data are shown at their respective values of H_b^{peak} for $L = 32$ (green) and 256 (blue). The corresponding values of the total applied field, $H(t) + H_b^{\text{peak}}$, are also shown in orange and magenta, respectively. The wave forms of $m(t)$, characteristic of single-droplet and multidroplet switching, are seen for $L = 32$ and 256, respectively.

dimensional Ising ferromagnet with only nearest-neighbor interactions, designed to closely mimic the experimental setup. At zero bias, such systems exhibit a dynamic phase transition (DPT) at a critical period P_c, where the period-averaged magnetization $\langle Q \rangle$ vanishes in a singular fashion. It has previously been shown that the DPT belongs to the equilibrium Ising universality class, with P playing the role of temperature and the bias H_b being the field conjugate to $\langle Q \rangle$. Following Riego *et al.* [17], we studied the dynamics of the system at values of P *above* P_c, and in agreement with the experiments we found that $\langle Q \rangle$ exhibits a strong bias dependence and fluctuation peaks at nonzero values of H_b, symmetrically located around zero bias.
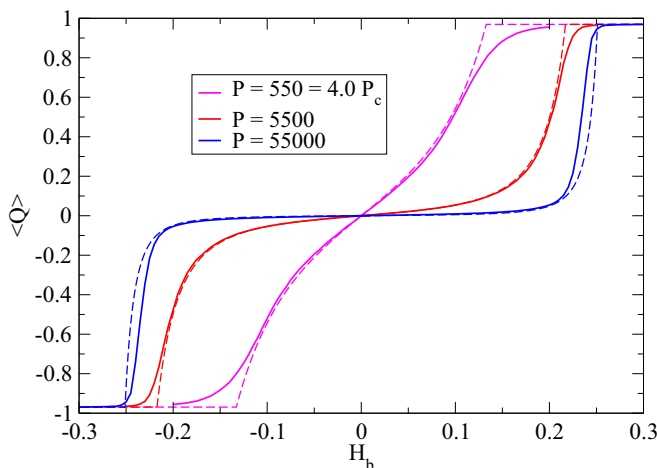

FIG. 7. Simulated results (solid) and approximate theoretical results from Eqs. (C1)–(C3) (dashed) for $\langle Q \rangle$ with a square-wave field of amplitude $H_0 = 0.3$. System size $L = 128$ and three different field periods P. In a square-wave field, $P_c \approx 137$ [7].

Since the simulated system has only nearest-neighbor interactions, our results show that the experimental results are *not* due to any residual magnetostatic interactions. The simulational approach also enables studies of the effects of finite system size. We found that, at fixed P, finite-size effects saturate beyond a P-dependent size limit. Using the droplet theory of magnetization switching, we conclude that this saturation occurs at the crossover between two different dynamic regimes. For small systems, the magnetization switching from the favored to the disfavored direction occurs by a stochastic single-droplet mechanism. For large systems, the switching occurs by the size-independent and nearly deterministic KJMA mechanism, which involves a large number of simultaneously nucleating and growing droplets. We therefore conclude that this "sideband" phenomenon for supercritical values of P is *not* a critical phenomenon, but rather a stochastic-resonance phenomenon. We believe these insights will be important for the design and analysis of devices that involve magnetization reversal by time-varying fields, such as memory elements, switches, and actuators.

APPENDIX A: MECHANISMS OF MAGNETIZATION REVERSAL

When a d-dimensional Ising ferromagnet below its critical temperature is subjected to the reversal of an applied field of magnitude $|H|$, the homogeneous nucleation rate per unit system volume for droplets of the new equilibrium phase is given by [6,18,20,28,30–32]

$$I(H) \approx B(T)|H|^K \exp\left[-\frac{\Xi_0(T)}{|H|^{d-1}}\right], \tag{A1}$$

where $B(T)$ is a nonuniversal function of T. For $d = 2$, $K = 3$, and $\Xi_0(0.8T_c) \approx 0.506$ (which includes a factor of $1/T$) [6]. The argument of the exponential function is the negative of the free energy of a critical droplet of the equilibrium phase, divided by T. The inverse of $L^d I(H)$ is the average time between random nucleation events for a system of size L.

Single-droplet reversal mechanism. Under conditions of small system and/or moderately weak field, the time it takes for the first nucleated droplet to grow to fill the system is much shorter than the average nucleation time. As a result, the magnetization reversal is completed by this single, first droplet [see Fig. 3(b)].

Multidroplet reversal mechanism. Under conditions of large system and/or moderately strong field, the average time between nucleation events is less than the time it would take the first nucleated droplet to grow to fill the system. Therefore, many droplets nucleate and grow independently in

different parts of the system until they coalesce and collectively fill the system [see Fig. 3(c)]. The result is a gradual and nearly deterministic growth of the new phase through a multidroplet process, well described by the KJMA approximation [18,24–28]. The characteristic reversal time is independent of the system size and given by

$$\langle \tau(H) \rangle \propto [v^d I(H)]^{-1/(d+1)}, \quad \text{(A2)}$$

where the propagation velocity of the droplet surface, v, is proportional to $|H|$ in this parameter range [33] as expected from the Lifshitz-Allen-Cahn approximation [34–36].

APPENDIX B: EXTREMELY LONG PERIODS

If the radius of the critical droplet reaches a size of about $L/2$, it will not fit in the $L \times L$ system, and a new regime, called the *coexistence regime*, is entered [18]. In this regime, the droplet is replaced by a slab of the equilibrium phase, and the nucleation time no longer depends on $|H|$, but increases exponentially with L^{d-1}. The critical droplet radius in d dimensions is given by [18],

$$R_c \approx \left(\frac{(d-1)T\,\Xi_0}{2m_0\Omega_d} \right)^{1/d} \frac{1}{|H|}, \quad \text{(B1)}$$

where Ω_d is the volume of the critical droplet, divided by R_c^d. Numerical values for the constants with $d = 2$ at $T = 0.8\,T_c \approx 1.815$ are found in Table I of Ref. [6]: $\Xi_0 \approx 0.506$ and $\Omega_2 \approx 3.152$. (The factor T is included in the numerator to cancel the factor $1/T$ in Ξ_0.) Thus we have

$$R_c \approx \frac{0.388}{|H|} \approx \frac{L}{2}. \quad \text{(B2)}$$

Replacing $|H|$ by $H_0 - |H_b|$ and setting $L = 32$, we thus find $1/(H_0 - |H_b|) \approx 41.3$. Finally, linearly extrapolating the large-P data for $L = 32$ in Fig. 5(b), we find that the single-droplet result from Eq. (10) should remain valid for periods up to approximately $10^{19 \pm 2}$. [The uncertainty in the exponent is the result of assuming a 10% uncertainty in the estimate of $1/(H_0 - |H_b|)$.] Beyond this limit, $H_0 - |H_b|$ should remain independent of P, at a value of $O(1/L)$. For larger L, the single-droplet result should be valid up to even longer periods. We do not expect that these extremely long periods should be of great experimental relevance for macroscopic systems. However, for nanoscopic systems the coexistence regime may be observable with experimentally accessible periods.

APPENDIX C: SQUARE-WAVE OSCILLATING FIELD

Now, instead of a sinusoidally oscillating field, consider a square-wave field, such that $H(t) = +H_0$ during one

half-period, and $-H_0$ during the other. Since the times that the total field is parallel and antiparallel to H_b now each equal $P/2$, the equivalent of the long-period, weak-bias approximation of Eq. (9) becomes $\langle Q \rangle \approx 0$. Therefore, the value of $\langle Q \rangle$ for finite P and weak H_b is determined by the difference between the average magnetization reversal times following a change of the total field from the favored to the disfavored direction, and the opposite. Since the total field now has its full favored or disfavored strength during the whole half-period, these average switching times will be shorter than the corresponding times in the sinusoidally oscillating field case. With a square-wave field of amplitude $H_0 = 0.3$ at $0.8T_c$ under Glauber dynamics, the critical period has been measured by MC simulations as $P_c \approx 137$ [7]. To calculate the transition times for a two-dimensional system in the multidroplet regime, we will again assume $H_b \geqslant 0$ for concreteness.

From Eqs. (A1) and (A2) with $|H| = H_0 - H_b$, we obtain the characteristic time scale for transitions from the favored (parallel to the bias field) to the disfavored magnetization direction, after the total applied field has changed sign as

$$t_{\text{FD}}(H_b, H_0) = \tau_0 \left(\frac{1}{1 - H_b/H_0} \right)^{5/3}$$
$$\times \exp\left(\frac{\Xi_0}{3H_0} \frac{H_b/H_0}{1 - H_b/H_0} \right) \geqslant \tau_0, \quad \text{(C1)}$$

where τ_0 is the magnetization reversal time for $H_b = 0$. Analogously, the switching time from the disfavored to the favored magnetization direction is

$$t_{\text{DF}}(H_b, H_0) = \tau_0 \left(\frac{1}{1 + H_b/H_0} \right)^{5/3}$$
$$\times \exp\left(-\frac{\Xi_0}{3H_0} \frac{H_b/H_0}{1 + H_b/H_0} \right) \leqslant \tau_0. \quad \text{(C2)}$$

Both t_{FD} and t_{DF} reduce to $\tau_0 \approx 74.6$ [6] for $H_b = 0$.

The order parameter $\langle Q \rangle$ is determined by P and the difference between t_{FD} and t_{DF} as

$$\langle Q \rangle \approx \begin{cases} 2m_0 \frac{t_{\text{FD}} - t_{\text{DF}}}{P} & \text{for} \quad t_{\text{FD}} \leqslant \frac{P}{2}, \\ m_0 & \text{for} \quad t_{\text{FD}} > \frac{P}{2}. \end{cases} \quad \text{(C3)}$$

This approximation is shown together with simulation results in Fig. 7. The agreement is very good for $|H_b| \lesssim |H_b^{\text{peak}}|$.

---

[1] T. Tomé and M. J. de Oliveira, Dynamic phase transition in the kinetic Ising model under a time-dependent oscillating field, Phys. Rev. A **41**, 4251 (1990).

[2] M. Rao, H. R. Krishnamurthy, and R. Pandit, Magnetic hysteresis in two model spin systems, Phys. Rev. B **42**, 856 (1990).

[3] W. S. Lo and R. A. Pelcovits, Ising model in a time-dependent magnetic field, Phys. Rev. A **42**, 7471 (1990).

[4] B. Chakrabarti and M. Acharyya, Dynamic transitions and hysteresis, Rev. Mod. Phys. **71**, 847 (1999).

[5] S. W. Sides, P. A. Rikvold, and M. A. Novotny, Kinetic Ising Model in an Oscillating Field: Finite-Size Scaling at the Dynamic Phase Transition, Phys. Rev. Lett. **81**, 834 (1998).

[6] S. W. Sides, P. A. Rikvold, and M. A. Novotny, Kinetic Ising model in an oscillating field: Avrami theory for the hysteretic

response and finite-size scaling for the dynamic phase transition, Phys. Rev. E **59**, 2710 (1999).

[7] G. Korniss, C. J. White, P. A. Rikvold, and M. A. Novotny, Dynamic phase transition, universality, and finite-size scaling in the two-dimensional kinetic Ising model in an oscillating field, Phys. Rev. E **63**, 016120 (2000).

[8] D. T. Robb, P. A. Rikvold, A. Berger, and M. A. Novotny, Conjugate field and fluctuation-dissipation relation for the dynamic phase transition in the two-dimensional kinetic Ising model, Phys. Rev. E **76**, 021124 (2007).

[9] G. M. Buendía and P. A. Rikvold, Dynamic phase transition in the two-dimensional kinetic Ising model in an oscillating field: Universality with respect to the stochastic dynamics, Phys. Rev. E **78**, 051108 (2008).

[10] H. Park and M. Pleimling, Dynamic phase transition in the three-dimensional kinetic Ising model in an oscillating field, Phys. Rev. E **87**, 032145 (2013).

[11] H. Fujisaka, H. Tutu, and P. A. Rikvold, Dynamic phase transition in a time-dependent Ginzburg-Landau model in an oscillating field, Phys. Rev. E **63**, 036109 (2001); **63**, 059903(E) (2001).

[12] R. A. Gallardo, O. Idigoras, P. Landeros, and A. Berger, Analytical derivation of critical exponents of the dynamic phase transition in the mean-field approximation, Phys. Rev. E **86**, 051101 (2012).

[13] O. Idigoras, P. Vavassori, and A. Berger, Mean field theory of dynamic phase transitions in ferromagnets, Physica B (Amsterdam) **407**, 1377 (2012).

[14] D. T. Robb and A. Ostrander, Extended order parameter and conjugate field for the dynamic phase transition in a Ginzburg-Landau mean-field model in an oscillating field, Phys. Rev. E **89**, 022114 (2014).

[15] D. T. Robb, Y. H. Xu, O. Hellwig, J. McCord, A. Berger, M. A. Novotny, and P. A. Rikvold, Evidence for a dynamic phase transition in [Co/Pt]$_3$ magnetic multilayers, Phys. Rev. B **78**, 134422 (2008).

[16] A. Berger, O. Idigoras, and P. Vavassori, Transient Behavior of the Dynamically Ordered Phase in Uniaxial Cobalt Films, Phys. Rev. Lett. **111**, 190602 (2013).

[17] P. Riego, P. Vavassori, and A. Berger, Metamagnetic Anomalies Near Dynamic Phase Transitions, Phys. Rev. Lett. **118**, 117202 (2017).

[18] P. A. Rikvold, H. Tomita, S. Miyashita, and S. W. Sides, Metastable lifetimes in a kinetic Ising model: Dependence on field and system size, Phys. Rev. E **49**, 5080 (1994).

[19] L. Gammaitoni, P. Hänggi, and P. Jung, Stochastic resonance, Rev. Mod. Phys. **70**, 223 (1998).

[20] S. W. Sides, P. A. Rikvold, and M. A. Novotny, Stochastic hysteresis and resonance in a kinetic Ising system, Phys. Rev. E **57**, 6512 (1998).

[21] G. Korniss, P. A. Rikvold, and M. A. Novotny, Absence of first-order transition and tricritical point in the dynamic phase diagram of a spatially extended bistable system in an oscillating field, Phys. Rev. E **66**, 056127 (2002).

[22] Ph. A. Martin, On the stochastic dynamics of Ising models, J. Stat. Phys. **16**, 149 (1977).

[23] E. Vatansever, Dynamically order-disorder transition in triangular lattice driven by a time dependent magnetic field, arXiv:1706.03351.

[24] A. N. Kolmogorov, A statistical theory for the recrystallization of metals, Bull. Acad. Sci. USSR, Phys. Ser. **1**, 355 (1937).

[25] W. A. Johnson and R. F. Mehl, Reaction kinetics in processes of nucleation and growth, Trans. Am. Inst. Mining and Metallurgical Engineers **135**, 416 (1939).

[26] M. Avrami, Kinetics of phase change, J. Chem. Phys. **7**, 1103 (1939); **8**, 212 (1940); **9**, 177 (1941).

[27] R. A. Ramos, P. A. Rikvold, and M. A. Novotny, Test of the Kolmogorov-Johnson-Mehl-Avrami picture of metastable decay in a model with microscopic dynamics, Phys. Rev. B **59**, 9053 (1999).

[28] K. Binder and P. Virnau, Overview: Understanding nucleation phenomena from simulations of lattice gas models, J. Chem. Phys. **145**, 211701 (2016).

[29] P. Riego, P. Vavassori, and A. Berger, Towards an understanding of dynamic phase transitions, Physica B (Amsterdam) (2017).

[30] J. S. Langer, Theory of the condensation point, Ann. Phys. (NY) **41**, 108 (1967).

[31] J. S. Langer, Statistical theory of the decay of metastable states, Ann. Phys. (NY) **54**, 258 (1969).

[32] N. J. Günther, D. A. Nicole, and D. J. Wallace, Instantons and the Ising model below T_c, J. Phys. A **13**, 1755 (1980).

[33] P. A. Rikvold and M. Kolesik, Analytic approximations for the velocity of field-driven Ising interfaces, J. Stat. Phys. **100**, 377 (2000).

[34] J. D. Gunton and M. Droz, *Introduction to the Theory of Metastable and Unstable States* (Springer-Verlag, Berlin, 1983).

[35] I. M. Lifshitz, Kinetics of ordering during second-order phase transitions, Zh. Eksp. Teor. Fiz. **42**, 1354 (1962) [Sov. Phys. JETP **15**, 939 (1962)] .

[36] S. M. Allen and J. W. Cahn, A microscopic theory for antiphase boundary motion and its application to antiphase domain coarsening, Acta Metall. **27**, 1085 (1979).